Conclusion: We have proposed an LAN with a reverse round robin service of the stations. The advantage of this scheme in comparison with other networks such as E-Net, is a better

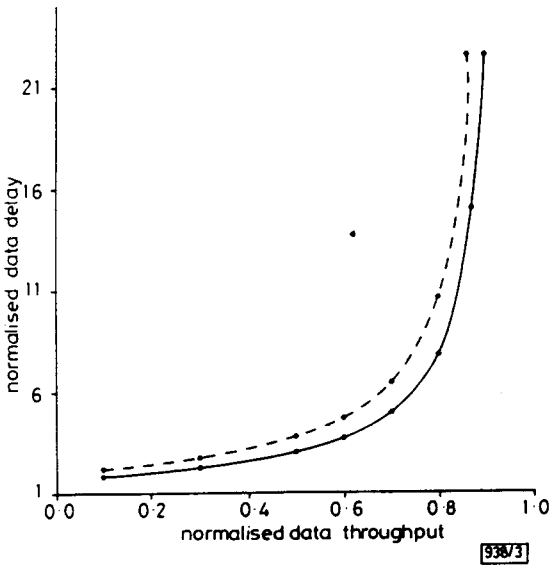

Fig. 3 *Data delay/data throughput characteristics, 100 Mbps*
---- E-Net
—— G-Net

delay performance. This characteristic makes our protocol particularly suitable for voice and data integration.

E. G. ECONOMOU
S. BOLIS

Department of Informatics
University of Athens
Panepistimiopolis, TYPA Building
157 71 Athens, Greece

3rd June 1991

References

1 'Token ring access method and physical layer specifications'. ANSI/IEEE std 802.5-1985 (ISO/IS 8802/5)
2 'Carrier sense multiple access with collision detection access method and physical layer specifications'. ANSI/IEEE std 802.3-1985 (ISO/IS 8882/3)
3 'Token passing bus access method and physical layer specifications'. ANSI/IEEE std 802.4-1985 (ISO/IS 8802/4)
4 TOBAGI, F., BORGONOVO, F., and FRATTA, L.: 'Expressnet: A high performance integrated services LAN', *IEEE J. Sel. Areas Commun.*, 1983, **SAC-1**, (5), pp. 898–913
5 ECONOMOU, E. G., BOLIS, S., and PHILOKYPROU, G.: 'FBC-Net: a reverse round robin LAN for voice and data traffic', *Comput. Commun.*, 1991, **14**, (1), pp. 44–52

539

PULSE REPETITION RATES IN PASSIVE, SELFSTARTING, FEMTOSECOND SOLITON FIBRE LASER

Indexing terms: Optical fibres, Lasers

Several unusual pulsing modes are observed in a selfstarting, passively mode-locked erbium fibre soliton laser capable of generating pulses with durations as short as 320 fs.

Rare-earth doped optical fibres offer wide gain bandwidths and provide an ideal medium for the generation of ultrashort optical pulses. To date, research in mode-locked fibre lasers has centred on active mode-locking schemes incorporating fast phase[1] and amplitude modulators.[2] However, the large nonlinear effects obtainable in optical fibres make passive mode-locking an attractive proposition. A selfstarting, passive mode-locking scheme based on the reflection properties of the nonlinear amplifying loop mirror (NALM)[3] has recently been reported.[4,5] The system is capable of both picosecond/nanosecond duration square pulse operation[4] and ultrashort femtosecond soliton generation.[5,6] We discuss the various modes of operation of the laser and present results on pulse repetition rates, an important characteristic for a practical source of ultrashort solitons.

The laser configuration is illustrated in Fig. 1. The switching characteristic of the NALM dictates that the minimum loss per cavity round-trip pulse shapes are either square pulses with a peak intensity determined by the switching power of the loop, or solitons. Both of these pulse forms can propagate

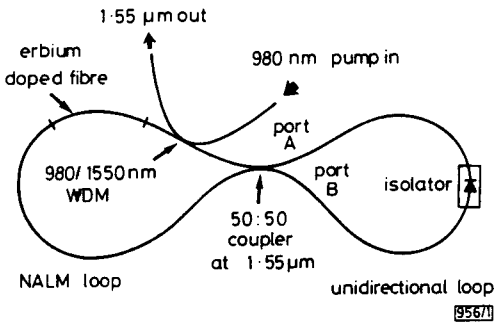

Fig. 1 *Experimental configuration of selfstarting, passively mode-locked fibre laser*

in a nonlinear medium with a constant phase across their entire envelope and this characteristic enables complete switching by the NALM.[7] To selfstart, noise is required at the NALM input to enable either the square or soliton pulse forms to develop. The noise is provided by reducing the linear cavity loss to a level sufficient for the onset of CW lasing. This is achieved either by applying a birefringence-induced phase bias within the NALM, or by arranging for asymmetric splitting at the NALM coupler. This latter option would permit the system to be constructed entirely of polarisation-maintaining fibre, thus improving system stability. Both square pulses with durations in the picosecond/nanosecond range[3] and femtosecond soliton pulses[4,5] have been observed experimentally with the system operating at 1·55 μm. The shortest pulses so far generated had a duration of 320 fs[4,5] and a corresponding time bandwidth product of 0·32. Fig. 2 shows a 600 fs pulse and its optical spectrum as an example. Note the two side lobes located 7 nm either side of the main peak. These features are always present when the laser enters the soliton regime and become progressively more pronounced as the soliton duration is reduced. The relative amplitude of the peaks can also vary enormously (see Reference 6). The origin of these lobes is not fully understood but could be a result of modulational instability.

As well as having two distinct modes of pulse generation, the system has at least three distinct regimes of operation with regard to pulse repetition rates. During square pulse operation (which constitutes the most stable operation of the

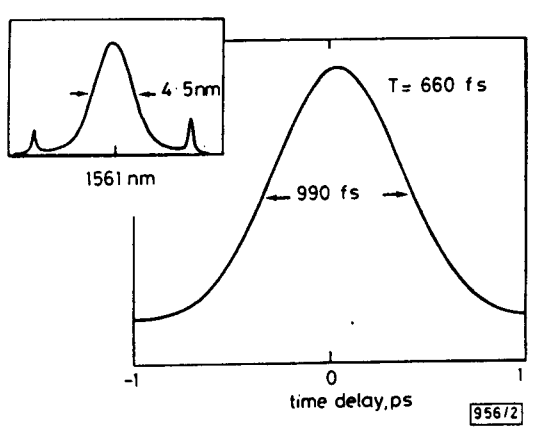

Fig. 2 *Background free autocorrelation trace and optical spectra of 660 fs soliton pulses*

system), pulses are generated at the cavity round-trip frequency. In this regime the repetition rate is stable with regard to changes in input pump power, provided that the pump power is not reduced to a level below which the pulsing cannot be sustained. The peak power of the square pulses remains clamped to the switching power of the NALM loop and, as the pump power to the system is increased, the extra power circulating in the cavity is taken up by a corresponding increase in pulse width.

The transition from the square pulse to the soliton regime of operation is most readily induced by changing the NALM phase bias. Three distinct modes of repetition rate behaviour have been observed. First, as the NALM phase bias is slowly altered, the square pulse is seen to break up into tightly-packed bunches of solitons, the bunches repeating at the cavity round-trip frequency. The situation is illustrated in Fig. 3. As the phase bias is adjusted close to the point at which the transition from square pulse to soliton behaviour occurs, large deviations from the expected 2 : 1 aspect ratio of the coherent spike to the pulse shoulder in the background free autocorrelation traces of the square pulses are observed. This observation indicates that the substructure on a femtosecond timescale develops within the square pulse just prior to the transition to the soliton regime. Pulse repetition rates as high as 100 GHz (as determined from autocorrelation scans) have been observed within the pulse bunches.

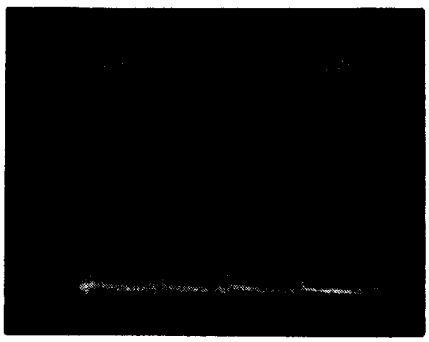

a

b

956/3

Fig. 3 *Soliton pulse bunches*

a Bunches circulating around cavity at cavity round trip frequency
b Exploded view of individual soliton bunch

Secondly the system can enter a soliton regime in which the solitons are no longer bunched, but occur seemingly randomly distributed over the entire cavity round-trip period, the pulse patterns repeating at the round-trip frequency. An example of this random pulsing is shown in Fig. 4*a*, where, because the detector response time (55 ps) is far longer than the pulse duration (500 fs), the trace effectively displays the pulse energy. The pulse with twice the amplitude of the others is caused by two pulses occurring within the detector response time and illustrates the quantisation of pulse energy associated with the fact that solitons are the preferred switching unit for system operation. Note that because of this energy quantisation, more pulses must circulate in the cavity if the pump power is increased, i.e. the average repetition rate must increase to obtain more output power. Moreover, no discernible change in the output soliton autocorrelation traces and spectra with pump power has been observed with the system. This is in contrast to the square pulse mode in which the pulse peak-intensity is clamped and increased circulating energy is taken up by an increase in pulse duration.

a

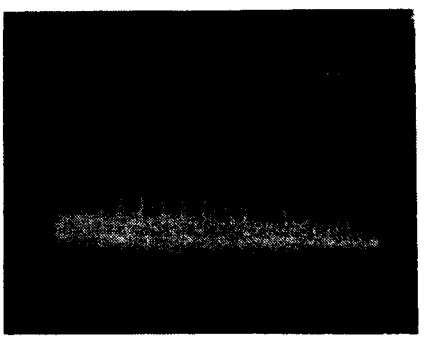

b

956/4

Fig. 4 *450 fs soliton pulse trains*

a Pulses randomly spaced but well separated
Pulse of apparently twice amplitude of others is due simply to two pulses arriving within time period less than detector response time
b Pure passive, harmonic mode-locking (f = 67·2 MHz, 16th harmonic of cavity round-trip frequency)

By appropriate adjustment of the pump power and birefringence of the NALM it is possible to enter the third pulse repetition rate regime and obtain pure harmonic mode-locking, as illustrated in Fig. 4*b*. However, in this mode the system is very sensitive to slight changes in pump power. Exactly what factors determine which of the three regimes of soliton generation is encountered are not yet fully understood. One possibility is that cross phase modulation between counterpropagating pulse bunches within the NALM loop can play a significant role in its switching operation. The effects of crossphase modulation would be minimised for tightly bunched pulse trains.

In conclusion, the various pulsing regimes of operation of the femtosecond soliton laser have been clarified. From a practical point of view, stabilisation of pulse repetition rates is an important goal. We have recently obtained encouraging results by incorporating within the system a pulse multiplier consisting of a recirculating fibre ring delay line.

D. J. RICHARDSON
R. I. LAMING
D. N. PAYNE
V. J. MATSAS
M. W. PHILLIPS

The Optoelectronics Research Centre
Southampton University
Southampton SO9 5NH, United Kingdom

5th June 1991

References

1 KAFKA, J. D., BAER, T., and HALL, D. W.: 'Mode-locked erbium fibre layer', *Opt. Lett.*, 1989, **14**, pp. 1269–1271
2 FERMANN, M. E., HOFER, M., HABERL, F., and CRAIG-RYAN, S. P.: 'Femtosecond fibre laser', *Electron. Lett.*, 1990, **26**, pp. 1737–1738
3 RICHARDSON, D. J., LAMING, R. I., and PAYNE, D. N.: 'Very low threshold Sagnac switch incorporating an erbium doped fibre amplifier', *Electron. Lett.*, 1990, **26**, pp. 1779–1781

4 RICHARDSON, D. J., LAMING, R. I., PAYNE, D. N., MATSAS, V. I., and PHILLIPS, M. W.: 'Selfstarting passively mode-locked fibre laser based on the amplifying Sagnac switch', *Electron. Lett.*, 1991, **27**, pp. 542–544
5 DULING III, I. N.: 'Subpicosecond all-fibre erbium laser', *Electron. Lett.*, 1991, **27**, pp. 544–545
6 RICHARDSON, D. J., LAMING, R. I., PAYNE, D. N., MATSAS, V. I., and PHILLIPS, M. W.: '320 fs soliton generation with passively mode-locked fibre laser', *Electron. Lett.*, 1991, **27**, p. 730–732
7 DORAN, N. J., and WOOD, D.: 'Non-linear optical loop mirror', *Opt. Lett.*, 1988, **13**, pp. 56–58

DEMONSTRATION OF HIGH PERFORMANCE HETEROJUNCTION FIELD EFFECT TRANSISTOR IN InAlAs/InGaAs/InAlGaAs/InP MATERIAL SYSTEM

Indexing terms: Field-effect transistors, Transistors, Semiconductor devices and materials

The heterojunction field effect transistor (HFET) is demonstrated for the first time in InAlAs/InGaAs/InAlGaAs/InP material system using molecular beam epitaxy (MBE). A tungsten gate selfaligned HFET structure was made by ion implantation and rapid thermal annealing. The 1·0 μm self-aligned gate HFET exhibited room temperature transconductance of 490 mS/mm with cutoff frequency of 9 GHz.

Introduction: The heterojunction field effect transistor (HFET) is a new type of field effect transistor proposed recently.[1] A feature of the device is that it is fabrication compatible with a variety of electronic and optoelectronic devices.[2] It is based on the concept of highly doped charge sheet, situated at the heterojunction interface, providing uniform and precisely controlled threshold voltage. The HFET was first demonstrated in an AlGaAs/GaAs material system[3] and has been shown to have high transconductance (510 mS/mm) and high speed (25 GHz).[4] We report the first *n*-channel HFET grown by MBE in an InAlAs/InGaAs/InAlGaAs/InP material system, lattice matched to semi-insulating InP substrate. This material system offers superior advantages over AlGaAs/GaAs material system, namely

(*a*) large conduction band discontinuity

(*b*) relatively higher electron mobility

(*c*) higher peak drift velocity in the device channel.

These properties translate into increased device transconductance and higher current gain cutoff frequency as has been demonstrated, in HEMTs[5] and HBTs[6] made in these material systems.

Device fabrication: The transistor structures were grown by MBE, lattice matched to 2 inch semi-insulating InP substrate. The MBE layers were as follows: 1000 Å of undoped $In_{0.52}Al_{0.48}As$ buffer layer, 1000 Å undoped $In_{0.53}Al_{0.21}Ga_{0.26}As$, 1000 Å of *P*-type ($5 \times 10^{16}$ cm^{-3}) $In_{0.53}Ga_{0.47}As$, 30 Å of undoped $In_{0.53}Al_{0.21}Ga_{0.26}As$ spacer, 50 Å of *N*-type (8×10^{18} cm^{-3}) $In_{0.53}Al_{0.21}Ga_{0.26}As$ charge layer, 30 Å of undoped $In_{0.53}Al_{0.21}Ga_{0.26}As$ spacer, 600 Å of *P*-type (1×10^{17} cm^{-3}) $In_{0.53}Al_{0.21}Ga_{0.26}As$ barrier layer, 400 Å of *P*-type (7×10^{18} cm^{v3}) $In_{0.52}Al_{0.48}As$. and 400 Å of *P*-type (1×10^{19} cm^{-3}) $In_{0.53}Ga_{0.47}As$ contact layer. Silicon and beryllium were used as *n* and *p*-type dopants, respectively. The important features of the growth structures are as follows: the n^+ charge layer is placed in InAlGaAs and sandwiched between two InAlGaAs spacer layers. The top spacer layer is used to prevent outdiffusion of Be into the charge layer. The bottom spacer layer separates the charge layer from the induced channel in the InGaAs surface at the heterointerface, thereby reducing ion scattering of the channel carriers. The last two layers, p^+-InAlAs and p^+-InGaAs, make a high-barrier gate contact to the induced carriers.

The individual devices were made by initially depositing 2000 Å of tungsten for the gate metal. A combination of photoresist and Al masking was used to pattern the tungsten by RIE; p^+-InGaAs, p^+-InAlAs, and *p*-InAlGaAs layers were etched using chemical assisted RIE down to the barrier layer, to form the gate. Silicon nitride was then used to form gate side walls, and was followed by silicon implant to form selfaligned source and drain. A single-step technique, involving ohmic contact resist mask, was used to etch InAlGaAs layers down to InGaAs layer to make recessed Ni/Au/Ge-alloyed ohmic contacts to the source and the drain. The completed device structure is shown in Fig. 1*a*.

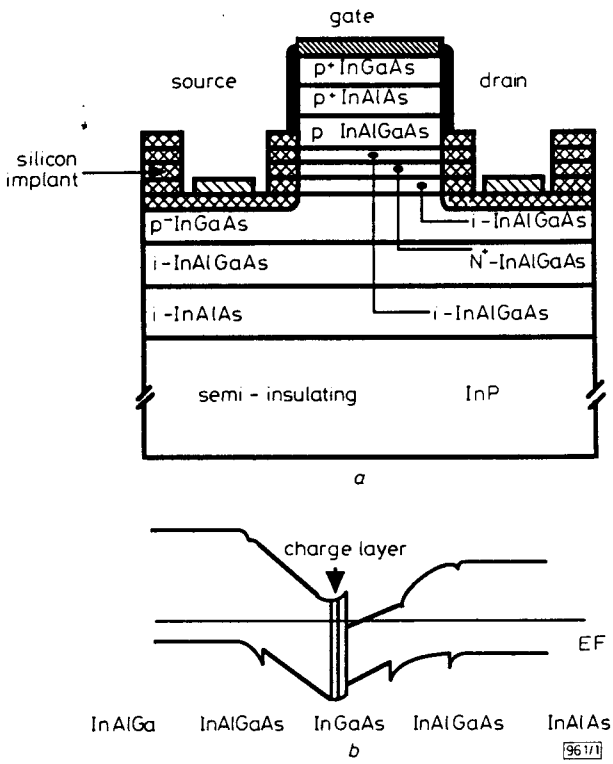

Fig. 1 *Schematic cross-section and energy band diagram of HFET*
a Schematic cross-section
b Energy band diagram of HFET

Results: Fig. 1*b*, shows the resulting energy band diagram. This Figure shows that the *n*-channel HFET is an inversion channel device in which the conducting channel resides in a *p*-type material. At zero gate bias no electron channel exists at the heterointerface. The device operates when the source is grounded and the gate is forward biased to induce the channel. Because the gate forms an ohmic contact to *p*-type semiconductor, larger gate voltages need to be applied before the gate conduction occurs. The channel conducts as the positive voltage on the drain is increased.

Typical room temperature output current–voltage characteristics of 1·0 μm gate length × 200 μm gate width HFETs are shown in Fig. 2. These characteristics show excellent saturation at 0·4 V. The threshold voltage was 0·9 V. The compression in the I–V characteristics with increasing gate voltage indicates a parallel conduction path exists in the InAlGaAs layers. At $V_{ds} = 3{\cdot}0$ V the saturation current is 11 mA (55 mA/mm). Fig. 3 shows the transconductance characteristics measured at $V_{ds} = 2{\cdot}0$ V. The maximum extrinsic transconductance was 490 mS/mm at $V_g = 1{\cdot}25$ V, which is comparable to that reported for the HFETs in AlGaAs/GaAs material system. The parallel conduction in the InAlGaAs is reflected in the transconductance characteristics, which shows parasitic transconductance of 5·5 mS for gate voltage of $V_g =$ 0–0·9 V, the onset of the inversion channel.

The *S* parameters of the HFETs were measured from 0·1–20 GHz using on-wafer probing techniques to obtain the device extrinsic unity current gain cutoff frequency f_T. The